Article

Not peer-reviewed version

MgAl Oxide Coatings Modified with CeO2 Particles Formed by Plasma Electrolytic Oxidation of AZ31 Magnesium Alloy: Photoluminescent and Photocatalytic Properties

Stevan Stojadinović * and Nenad Radić

Posted Date: 6 March 2024

doi: 10.20944/preprints202403.0154.v1

Keywords: plasma electrolytic oxidation; photocatalysis; photoluminescence, MgO, MgAl2O4, methyl orange

 doi:10.20944/preprints202403.0154.v1

Article

MgAl Oxide Coatings Modified with CeO_2 Particles Formed by Plasma Electrolytic Oxidation of AZ31 Magnesium Alloy: Photoluminescent and Photocatalytic Properties

Stevan Stojadinović [1,2,*] and Nenad Radić [3]

[1] Faculty of Physics, University of Belgrade, Studentski trg 12–16, Belgrade, Serbia
[2] Faculty of Forestry, University of Belgrade, Kneza Višeslava 1, Belgrade, Serbia
[3] IChTM—Department of Catalysis and Chemical Engineering, University of Belgrade, Njegoševa 12, Belgrade, Serbia; nradic@nanosys.ihtm.bg.ac.rs
* Correspondence: sstevan@ff.bg.ac.rs; Tel.: +381-11-7158161

Abstract: MgAl oxide coatings containing MgO and $MgAl_2O_4$ phases were doped with CeO_2 particles using plasma electrolytic oxidation (PEO) of AZ31 magnesium alloy in 5 g/L $NaAlO_2$ water solution, with CeO_2 particles added at concentrations up to 8 g/L. They underwent extensive investigation into their morphology, chemical and phase compositions, and most importantly, photoluminescent (PL) properties and photocatalytic-activity (PA) in photodegradation of methyl orange (10 cm^3 of 8 mg/L). The concentration of CeO_2 particles in the aluminate electrolyte influences the amount of CeO_2 particles incorporated into MgAl oxide coatings, but CeO_2 particles have no signi-ficant effect on the surface morphology, thickness, or phase structure of the coatings. The PL emi- ssion spectrum of MgAl oxide coating is divided into two bands: one in the 350-600 nm range related to structural defects in MgO, and another much more intense in the 600-775 nm range attributed to F^+ centres in $MgAl_2O_4$. Incorporated CeO_2 particles do not have a significant effect on the PL intensity of the band in the red spectral region, but the PL intensity of the first band increases with the concentration of CeO_2 particles. PA of MgAl/CeO_2 oxide coatings is higher than that of pure MgAl oxide coatings. The highest PA was observed for MgAl/CeO_2 oxide coatings formed in aluminate electrolytes with the addition of 2 g/L of CeO_2 particles. The MgAl/CeO_2 oxide coatings remained chemically and physically stable across multiple cycles, indicating their potential for applications.

Keywords: plasma electrolytic oxidation; photocatalysis; photoluminescence; MgO; $MgAl_2O_4$; methyl orange

1. Introduction

Plasma electrolytic oxidation (PEO) is an eco-friendly electrochemical surface treatment technique that produces highly stable oxide coatings on a variety of metals (Mg, Al, Ti, Ta, Nb, Zr) and their alloys with high crystallinity, substrate adhesion, and physical, chemical, and thermal stability [1–4]. PEO necessitates high anodic voltage (several hundred volts) to promote the local dielectric breakdown of the growing oxide film, resulting in numerous short-lived micro-discharges generated continuously over the metal electrode surface [5]. The breakdown process entails intricate electrochemical, thermal, and plasma processes that incorporate both metal and electrolyte components into coatings.

Magnesium and magnesium alloys are desirable materials for practical applications due to their low density, high strength-to-weight ratio, excellent dimensional stability, biodegradability and biocompatibility, large hydrogen storage capacity, high specific capacity for batteries, good

 doi:10.20944/preprints202403.0154.v1

electromagnetic shielding, high machinability, and so on [6,7]. The main drawback of magnesium-based materials is their poor resistance to corrosion which limits their application [8]. Surface modification of magnesium and its alloys is commonly used to improve their anti-corrosion properties and create functional coatings for a variety of applications [9].

In recent years, PEO has become a popular method for improving the surface properties of magnesium and its alloys and forming multifunctional coatings [10–18]. Some studies have shown that oxide coatings formed on magnesium alloys can be used in photocatalytic applications [19–23]. The present study focuses on the investigation of photoluminescent (PL) and photocatalytic properties of coatings formed by PEO of AZ31 magnesium alloy in aluminate electrolyte with the addition of CeO_2 particles in different concentrations. PEO coatings formed on AZ31 magnesium alloy in aluminate electrolytes containing MgO and $MgAl_2O_4$ phases [22]. Both of these phases have found application in photocatalysis [24,25] and as hosts for photoluminescence materials [26,27] due to the presence of various kinds of oxygen vacancies and other defects.

Adding CeO_2 particles to the electrolyte causes their incorporation into the coatings during PEO on magnesium alloys, which improves their corrosive properties [28,29]. The main idea behind this work was to create $MgO/MgAl_2O_4/CeO_2$ coatings in order to improve the photocatalytic and PL properties of a single $MgO/MgAl_2O_4$ coating and optimize the amount of CeO_2 particles in the electrolyte. The properties of CeO_2 such as its low toxicity, strong oxygen storage capacity, high chemical stability, and ability to display dual oxidation states of cerium, Ce^{3+}/Ce^{4+}, have drawn a lot of attention in the field of photocatalysis due to the formation of abundant oxygen vacancies in CeO_2, which serve as active electron trap centres, inhibiting recombination of photo-generated electron/hole pairs [30–34].

The photocatalytic and PL properties of the MgO/CeO_2 and $MgAl_2O_4/CeO_2$ systems have received little attention in the literature [35–37], with no data available for the $MgO/MgAl_2O_4/CeO_2$ system. Consequently, in this study, the $MgO/MgAl_2O_4/CeO_2$ coatings formed by PEO were characterized using SEM/EDS, XRD, Raman spectroscopy, and DRS to investigate the effect of CeO_2 on the morphology, chemical composition, crystal structure, and absorption properties of $MgO/MgAl_2O_4/CeO_2$. The PL of the $MgO/MgAl_2O_4/CeO_2$ coatings was thoroughly investigated, as the incorporation of CeO_2 into $MgO/MgAl_2O_4$ coatings increases the PL intensity by more than an order of magnitude. Methyl orange (MO) dye was used to test the photocatalytic properties of the formed coatings. MO is an example of a typical azo-anionic dye, which is hard to degrade, hazardous to the environment, and potentially dangerous to human health if it finds its way into the soil and water resources.

2. Materials and Methods

The starting material for the of preparation PEO coatings was a rectangular sample of AZ31 magnesium alloy (96% Mg, 3% Al, 1% Zn, Alfa Aesar) with dimensions of 25 mm × 10 mm × 0.81 mm. Samples preparation for PEO includes their ultrasonic cleaning with acetone and dried in a warm air stream. Subsequently, insulating resin was applied to the samples, exposing only the 15 mm × 10 mm active surface to the electrolyte.

The electrolytic cell was made of double-walled glass and cooled with water (refer to Figure 10 in Ref. [22]). To ensure that particles were distributed evenly in the electrolytic cell, the electrolyte was stirred with a magnetic stirrer. The tubular stainless-steel cathode was positioned around the anode samples of AZ31 magnesium alloy, which were used, and positioned in the centre of the electrolytic cell. The electrolytic solution was prepared using 5 g/L $NaAlO_2$ in distilled water with the addition of CeO_2 particles in concentrations ranging from 1 g/L to 8 g/L. The PEO processes were performed using a DC power source (Consort EV261) at a constant current density of 150 mA/cm^2 and treated for 10 min. The electrolyte was kept at a temperature of (20 ± 1) ^{o}C. Samples were rinsed in distilled water after the PEO to inhibit additional electrolyte component deposition during drying.

The morphology, thickness, elemental and phase analysis of the PEO coatings were performed using a scanning electron microscope (SEM, JEOL 840A, Tokyo, Japan) with energy-dispersive X-ray spectroscopy (EDS, Oxford INCA, Abingdon, UK), X-ray diffraction (XRD, Rigaku Ultima IV, Tokyo,

 doi:10.20944/preprints202403.0154.v1

Japan), and Raman spectroscopy (TriVista 557 Raman system, S&I GmbH, Germany). The optical properties of the PEO coatings were examined by UV-Vis diffuse reflectance spectra (DRS, Shimadzu UV-3600, Tokyo, Japan). Room temperature PL excitation and emission spectra were acquired by spectrofluorometer (Horiba Jobin Yvon, Fluorolog FL3-22, Edison, NJ, USA) with a 450 W xenon lamp as the excitation source.

The photodegradation of MO, the model compound for organic pollution, was investigated at 20 °C under artificial solar radiation in order to assess the photocatalytic activity (PA) of the coatings that were formed. The photocatalytic reactor was a double-walled glass with water cooling (refer to Figure 1 in Ref. [38]). The samples were positioned on the stainless steel holder 5 mm above the bottom of the photocatalytic reactor. A magnetic stirrer that was positioned underneath the holder was used to mix the 10 cm^3 solution of MO. The MO concentration was 8 mg/L at first. A 300 W lamp (OSRAM ULTRA-VITALUX UV-A, Germany) placed 25 cm above the solution's upper surface was used to illuminate the samples. To reach adsorption-desorption equilibrium, the initial MO solution and samples were left in the dark for an hour prior to illumination. By measuring the MO decomposition after a suitable time of light exposure, PA was ascertained. A UV-Vis spectrometer (Thermo Electron Nicolet, Evolution 500, UK) was used to measure the maximum MO absorption peak at 464 nm. Using a standard curve that demonstrated a linear relationship between concentration and absorbance at this wavelength, the absorbance was converted to MO concentration.

3. Results and discussion

Figure 1 displays the top view and cross-section SEM micrographs of the coating created in 5 g/L $NaAlO_2$ with the addition of CeO_2 particles at different concentrations. Changing the concentration of CeO_2 particles has no discernible effect on the surface morphology or coating thickness. All coatings share a common morphology defined by the presence of molten regions dispersed throughout the surface created when the molten oxide heats up, melts, and then cools down in contact with the surrounding electrolyte and pores formed as a result of gas bubbles released during the PEO [39]. The coatings formed after 10 minutes of PEO are about (22 ± 1) μm thick.

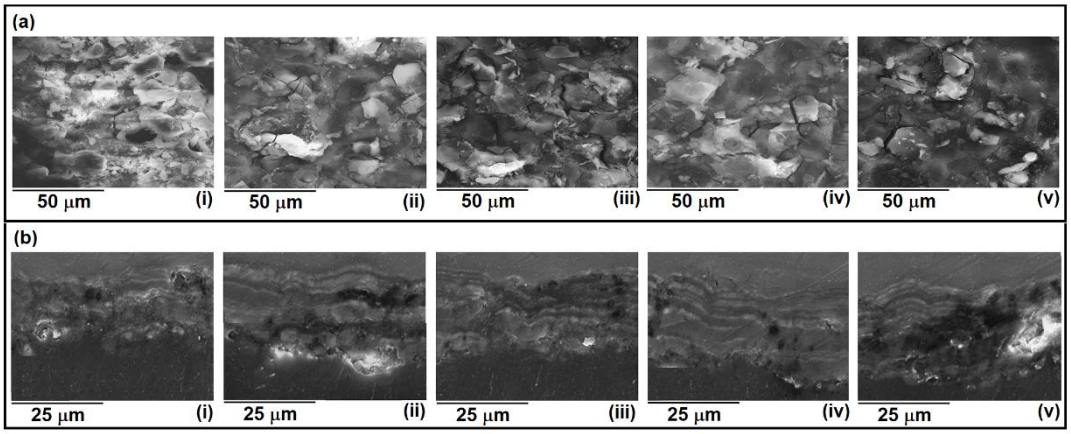

Figure 1. (**a**) Top view; (**b**) cross-section; micrographs of coatings formed in 5 g/L $NaAlO_2$ with the addition of CeO_2 particles in concentration: (i) 0 g/L; (ii) 1 g/L; (iii) 2 g/L; (iv) 4 g/L; (v) 8 g/L.

Integrated EDS analysis of coatings is given in Table 1 (the relative errors are less than 5%). The coatings' chemical constituents are Mg, Al, O, and Ce. Electrolyte is the main source of Al. Small amounts of Ce are present in coatings, which increase with the concentration of CeO_2 particles in the electrolyte.

 doi:10.20944/preprints202403.0154.v1

Table 1. Integrated EDS analysis of coatings in Figure 1a formed in 5 g/L $NaAlO_2$ with the addition of CeO_2 particles at different concentrations.

CeO_2 (g/L)	Atomic (%)			
	O	Mg	Al	Ce
0	65.44	14.02	20.54	/
1	65.53	14.79	19.63	0.05
2	64.52	15.76	19.61	0.11
4	64.84	15.91	19.02	0.23
8	64.43	15.85	19.32	0.40

The XRD patterns of PEO coatings formed in 5 g/L $NaAlO_2$ with different concentrations of CeO_2 particles added, along with the XRD pattern of pure CeO_2 particles and AZ31 magnesium alloy substrate, are displayed in Figure 2a. The peaks observed in XRD patterns of CeO_2 particles at 2θ values of 28.7, 33.2, 47.6, 56,4, 59.2, 69.5, 76.8 and 79.2 degrees, correspond to the (111), (200), (220), (311), (222), (400), (331), and (420) crystalline planes of cubic fluorite structure of CeO_2 (JCPDS Card No. 75-0162). The formation of MgO (JCPDS card No. 79-0612) and $MgAl_2O_4$ (JCPDS card No. 77-0435) phases, as a result of an interaction between the AZ31 substrate and the electrolyte components, are indicated by the XRD pattern of PEO coating formed in 5 g/L $NaAlO_2$ [22]. The X-ray penetration through the porous oxide layer and reflection of the substrate makes diffraction peaks from the substrate significant. The diffraction peaks of CeO_2 can be clearly seen together, with the diffraction peaks arising from MgO and $MgAl_2O_4$ in the XRD patterns of the PEO coatings formed in 5 g/L $NaAlO_2$ with the addition of a high concentration of CeO_2 particles (4 g/L and 8 g/L). This is primarily due to the low concentration of evenly distributed CeO_2 particles throughout the surface coatings.

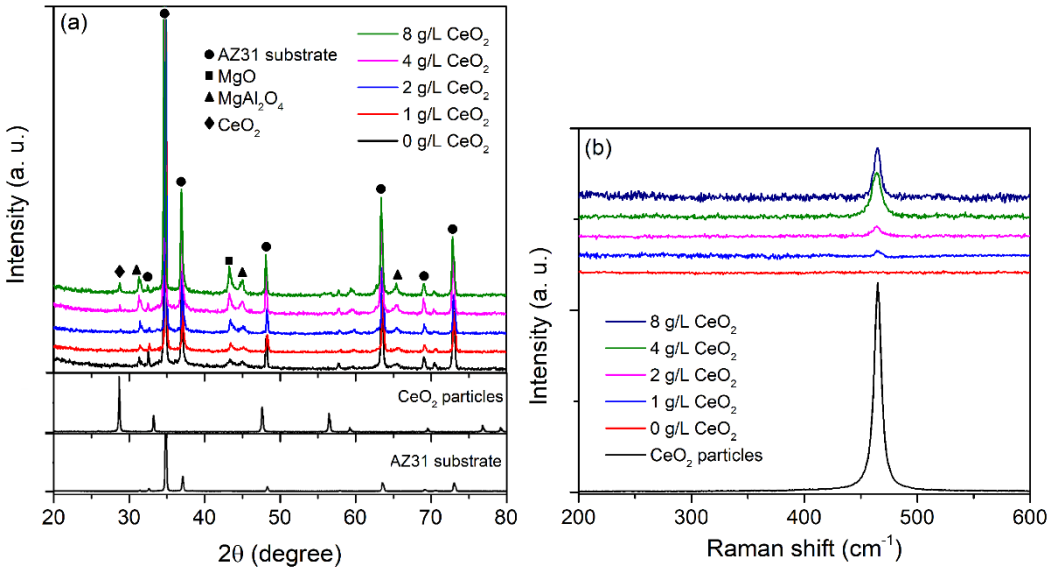

Figure 2. (**a**) XRD patterns; (**b**) Raman spectra; of coatings formed in 5 g/L $NaAlO_2$ with addition of CeO_2 particles in different concentrations.

To verify that CeO_2 particles are also present in PEO coatings formed in 5 g/L $NaAlO_2$ with the addition of lower concentrations of CeO_2 particles (1 g/L and 2 g/L), we conducted Raman measurements (Figure 2b). The Raman spectrum of CeO_2 particles exhibits a prominent band located approximately at 465 cm^{-1}, identified as the F_{2g} mode of the cubic fluorite structure of CeO_2 attributed to the symmetrical vibration of oxygen atoms surrounding the Ce^{4+} [40]. This mode can be found on the Raman spectra of all coatings formed in 5 g/L $NaAlO_2$ with the addition of CeO_2 particles, indicating that CeO_2 particles were incorporated into the coatings.

 doi:10.20944/preprints202403.0154.v1

During PEO, particles from the electrolyte can be incorporated into the coatings in three ways: reactive, partly reactive, and inert [41]. The melting point and particle size are the two most important factors in determining the incorporation mode. Particles with a high melting point, such as CeO_2 (around 2400 °C), are distinguished by an inert mode of incorporation [42], which also applies to our case.

PL excitation and emission spectra of MgO/$MgAl_2O_4$ coating are shown in Figure 3. The PL emission spectrum excited at 265 nm (Figure 3a) is characterized by a strong emission band in a red region with a maximum at about 720 nm which is associated with F^+ centres in $MgAl_2O_4$ [43] and a broad band in the range from 350 nm to 600 nm which is associated with oxygen vacancies (e.g. F, F^+, F_2, and F_2^{2+} centres), mostly in MgO [44,45]. Upon excitation with 340 nm (Figure 3b), two PL bands with peak positions at about 410 nm and 660 nm can be observed in the PL emission spectrum, which is related to oxygen vacancies in MgO [46].

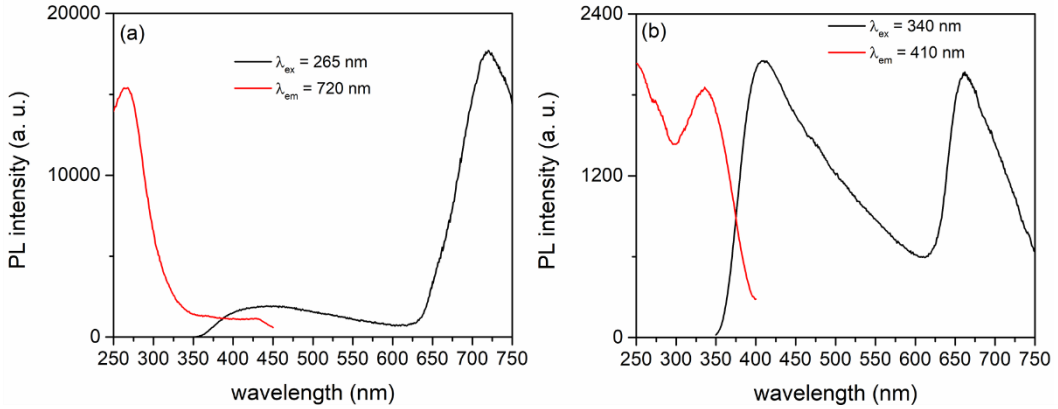

Figure 3. PL excitation and emission spectra of MgO/$MgAl_2O_4$ coating: (**a**) λ_{ex} = 265 nm, λ_{em} = 720 nm; (**b**) λ_{ex} = 340 nm, λ_{em} = 410 nm.

Under 265 nm excitation PL intensity of the band with a maximum at about 720 nm is not significantly affected by the incorporation of CeO_2 particles to the MgO/$MgAl_2O_4$ coatings, but the PL intensity of the broad band with a maximum at about 410 nm is significantly increased (Figure 4a). PL emission spectra excited at 340 nm also show that the PL intensity of the band with a maximum of about 410 nm increases with the increase in the concentration of CeO_2 particles incorporated in the MgO/$MgAl_2O_4$ coatings (Figure 4b). The ratio of the PL intensity of the coatings formed in 5 g/L $NaAlO_2$ with the addition of 8 g/L CeO_2 particles and without is about 20. In addition to this PL band, a PL band with a maximum at around 520 nm as well as PL bands in the red region of weak PL intensity can be observed in the PL emission spectra (Figures 4a,b).

PL excitation spectra monitored at 720 nm of MgO/$MgAl_2O_4$/CeO_2 coatings consist of one intense band with a maximum of about 265 nm (Figure 4c). The content of CeO_2 in the MgO/$MgAl_2O_4$/CeO_2 coatings does not affect the PL intensity of this band, which is in agreement with the corresponding PL emission spectra in Figure 3a. PL excitation spectra monitored at 410 nm and 520 nm of MgO/$MgAl_2O_4$/CeO_2 coatings consist of at least three bands at about 265 nm, 315 nm, and 340 nm. The transition at 340 nm is the most intense of these excitation transitions.

The increase in the PL intensity of MgO/$MgAl_2O_4$/CeO_2 coatings compared to pure MgO/$MgAl_2O_4$ is due to the creation of oxygen vacancies as a result of the incorporation of CeO_2 because PL originating from CeO_2 particles is negligible. Bands with maxima at around 410 nm and 520 nm are attributed to F^+ and F centres, respectively [47–49].

Preprints.org (www.preprints.org) | NOT PEER-REVIEWED | Posted: 6 March 2024 doi:10.20944/preprints202403.0154.v1

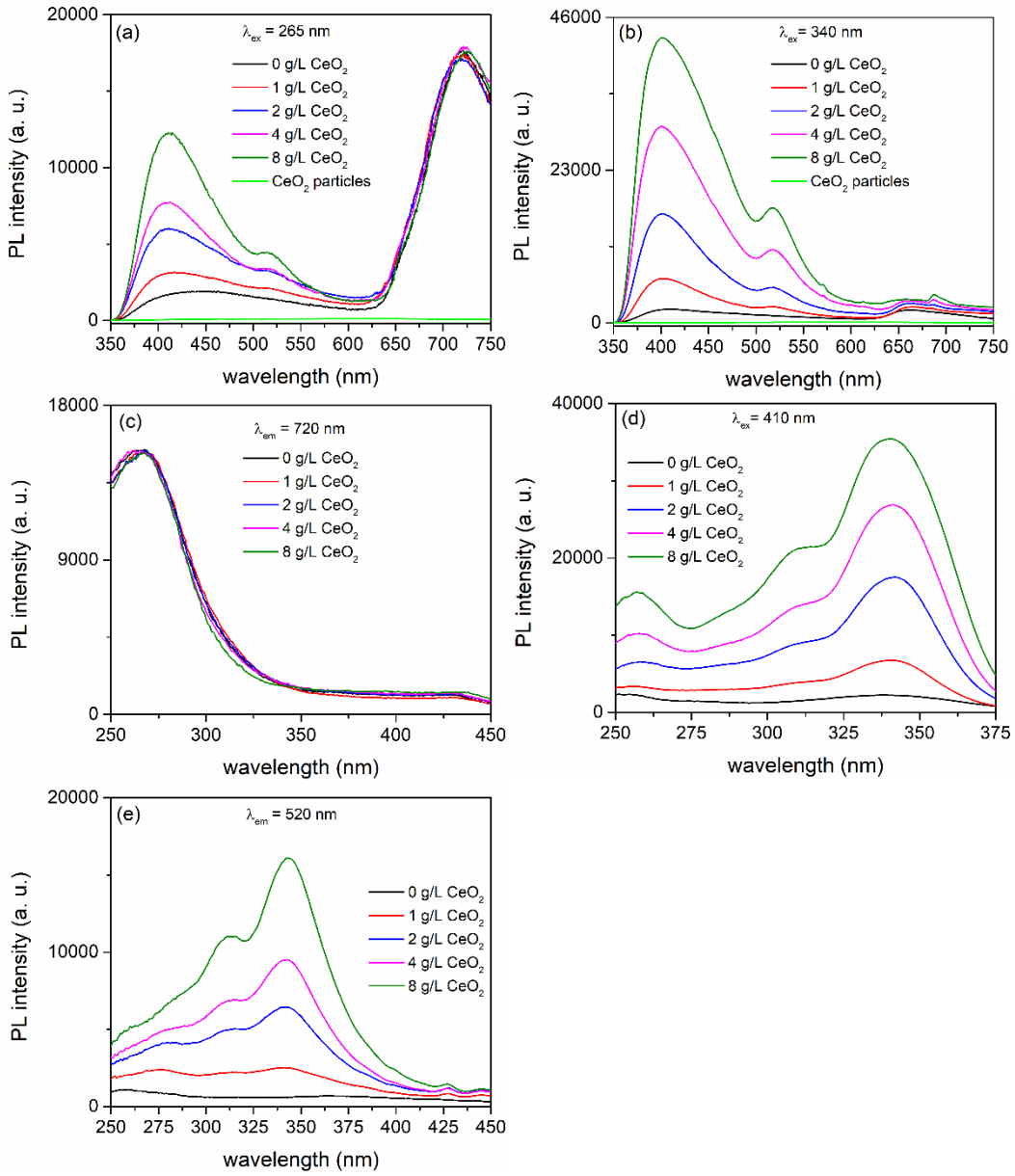

Figure 4. PL spectra of $MgO/MgAl_2O_4/CeO_2$ coatings formed in 5 g/L $NaAlO_2$ with the addition of CeO_2 particles in different concentrations: (**a**) emission spectra excited with 265 nm; (**b**) emission spectra excited with 340 nm; (**c**) excitation spectra monitored at 720 nm; (**d**) excitation spectra monitored at 410 nm; (**e**) excitation spectra monitored at 520 nm. .

Figure 5a illustrates how the concentration of CeO_2 particles in the electrolyte affects the MO photodegradation efficiency using the formed coatings. C_0 is the initial concentration of MO, and its concentration at time t is C. For every CeO_2 concentration, three samples were examined and the mean values are displayed in Figure 5a. Samples collected under identical conditions have very high reproducibility (within 3%) for the PA. The concentration of CeO_2 particles added to the electrolyte affects the PA of $MgO/MgAl_2O_4/CeO_2$ coatings, which is significantly higher than that of $MgO/MgAl_2O_4$ coating. The highest PA of $MgO/MgAl_2O_4/CeO_2$ coatings was achieved with the addition of 2 g/L of CeO_2 particles.

The first-order kinetic Langmuir Hinshelwood model (Figure 5b) provides a good description of the photocatalytic degradation of MO:

$$ln\left(\frac{C_o}{C}\right) = k_{app}t \quad (1)$$

Preprints.org (www.preprints.org) | NOT PEER-REVIEWED | Posted: 6 March 2024 doi:10.20944/preprints202403.0154.v1

The first-order kinetic constant k_{app}, determined by non-linear least squares fitting over the whole experimental time range [50], is provided in Table insert in Figure 6b, along with the corresponding standard squared deviation (σ) and linear correlation coefficient (R^2). As the concentration of CeO_2 particles in the aluminate electrolyte increased up to 2 g/L, the degradation rate constant k_{app} increased from 0.0809 h^{-1} to 0.1273 h^{-1}. The sensitivity of MO degradation on the content of CeO_2 in $MgO/MgAl_2O_4/CeO_2$ coatings was confirmed by a decrease in the degradation rate constant observed when the concentration of CeO_2 in aluminate electrolyte increased up to 8 g/L.

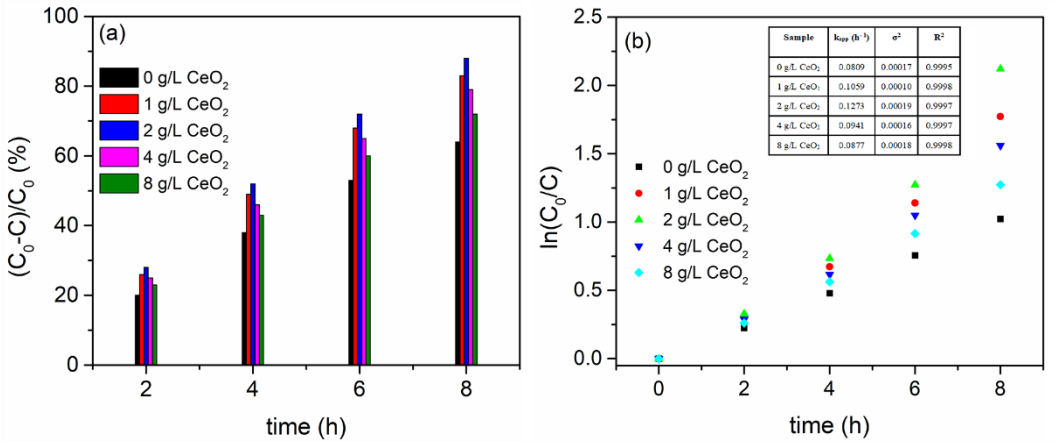

Figure 5. (**a**) PA; (b) First-order kinetic plots of coatings formed in 5 g/L $NaAlO_2$ with addition of CeO2 particles in different concentrations.

CeO_2 particles have a very low PA in organic dye degradation due to the rapid recombination of photo-generated electron-hole pairs [51]. Because the concentration of CeO_2 particles in the formed $MgO/MgAl_2O_4/CeO_2$ coatings is so low, the contribution of CeO_2 particles to the total PA of these coatings is negligible. Since the morphology, thickness, and phase structure of all formed coatings are essentially the same (Figures 1, 2), CeO_2 particles can contribute to increase the PA of $MgO/MgAl_2O_4$ coating primarily by broadening the optical absorption range of $MgO/MgAl_2O_4/CeO_2$ coatings or by slowing down the fast recombination of photo-generated electron/hole pairs.

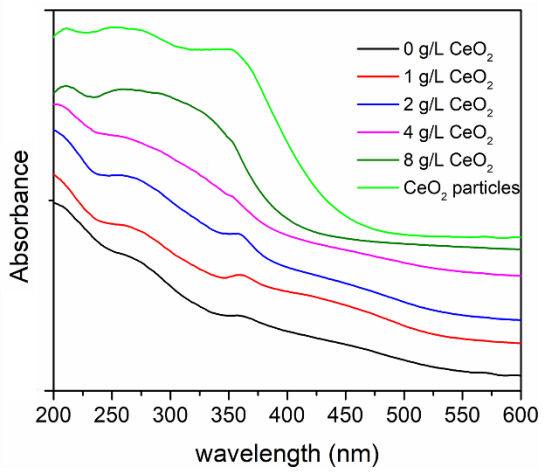

Figure 6. DRS spectra of CeO_2 particles and coatings formed in 5 g/L $NaAlO_2$ with the addition of CeO_2 particles in different concentrations.

UV–Vis DRS spectra of CeO_2 particles and formed coatings are shown in Figure 6. A broad absorption band in the mid-UV region is typical for $MgO/MgAl_2O_4$ formed in aluminate electrolyte [22]. The used CeO_2 particles have an absorption band-edge at about 440 nm. Due to the low concentration of CeO_2 in the formed coatings, the shift of the absorption curves towards the visible region is insignificant, especially for low concentrations of CeO_2 particles in the electrolyte (1, 2, and

 doi:10.20944/preprints202403.0154.v1

4 g/L). This indicates that the increased PA of $MgO/MgAl_2O_4/CeO_2$ coatings compared to $MgO/MgAl_2O_4$ coating is due to a decrease in photo-generated electron/hole recombination rate as a result of $MgO/MgAl_2O_4$ and CeO_2 coupling.

PL and PA measurements indicate that the high concentration of various types of oxygen vacancies and other defects in the formed coatings are related to the significant PA of $MgO/MgAl_2O_4/CeO_2$ coatings. The formation of oxygen vacancies during PEO introduces the defect states within the material's bandgap facilitating photo-generated charge carrier separation which leads to an increase in PA of $MgO/MgAl_2O_4/CeO_2$ coatings formed in aluminate electrolyte with the addition of CeO_2 particles in relation to $MgO/MgAl_2O_4$ coating formed in pure aluminate electrolyte. The PA of $MgO/MgAl_2O_4/CeO_2$ coatings is influenced by the concentration of CeO_2 particles added to the aluminate electrolyte. The $MgO/MgAl_2O_4/CeO_2$ coating, which was formed in the aluminate electrolyte with the addition of 2 g/L CeO_2 particles, had the highest PA. As the concentration of CeO_2 particles in the aluminate electrolyte increases, the PA decreases because CeO_2 particles serve as photo-induced electron capture centers [52].

Ten consecutive photocatalytic tests were conducted on the most active photocatalyst in order to investigate the potential application of $MgO/MgAl_2O_4/CeO_2$ coatings in photocatalysis. Figure 7 shows the recycling test of MO photo-degradation as well as morphology and compositions before and after 10 runs. The morphology, composition and PA did not change, suggesting that the produced photocatalyst had a high degree of chemical and physical stability .

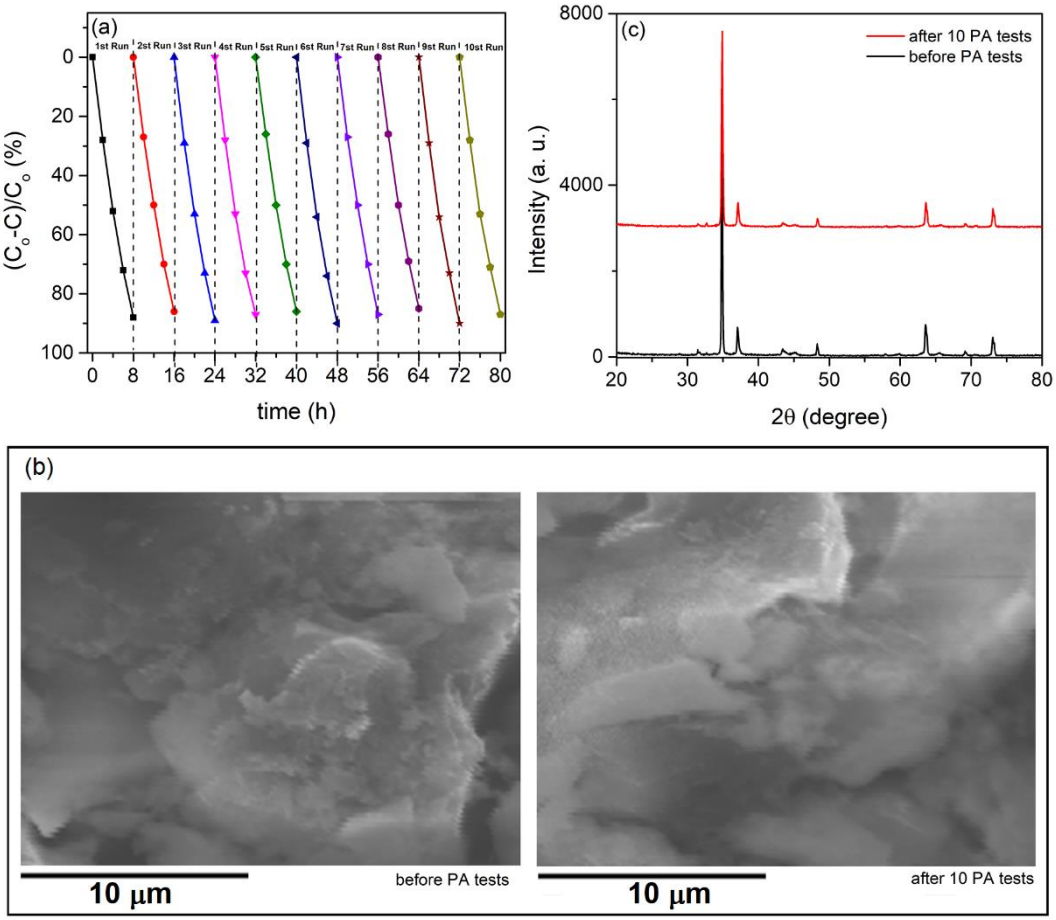

Figure 7. (**a**) Recycling test of MO photodegradation; (**b**) SEM micrographs before and after 10 cycles; (**c**) XRD patterns before and after 10 cycles; of coating formen in in 5 g/L $NaAlO_2$ + 2 g/L CeO_2.

 doi:10.20944/preprints202403.0154.v1

4. Conclusions

PEO of AZ31 magnesium alloy in aluminate, with additions of CeO_2 particles at varying electrolytes, was used to create $MgO/MgAl_2O_4/CeO_2$ coatings. To examine the morphology, crystal structure, chemical composition, optical, and PL properties of the formed coatings, various techniques including SEM/EDS, XRD, Raman spectroscopy, XPS, DRS, and PL were utilized. The potential of $MgO/MgAl_2O_4/CeO_2$ coatings for photocatalysis was evaluated by observing the photo-degradation of MO under simulated sunlight.

The following results can be drawn:

- The surface morphology, thickness, phase structure, and optical absorption of all formed coatings are not significantly affected by the addition of CeO_2 particles to the aluminate electrolyte.
- As a result of the incorporation of CeO_2 in coatings during PEO, oxygen vacancies are created, which accounts for the increase in PL intensity of $MgO/MgAl_2O_4/CeO_2$ coatings over pure $MgO/MgAl_2O_4$ coating because PL originating from CeO_2 particles is barely noticeable.
- The concentration of CeO_2 particles in the aluminate electrolyte, i.e. the amount of CeO_2 particles incorporated into $MgO/MgAl_2O_4$ coatings, determines the PA of $MgO/MgAl_2O_4/CeO_2$ coatings. The decrease in photo-generated electron/hole recombination rate resulting from $MgO/MgAl_2O_4$ and CeO_2 coupling is linked to the increased PA of $MgO/MgAl_2O_4/CeO_2$. The $MgO/MgAl_2O_4/CeO_2$ coating, which was formed in the aluminate electrolyte with the addition of 2 g/L CeO_2 particles, exhibits the highest PA.
- The PA, morphology, and compositions of the formed photocatalysts did not alter after multiple PA cycles, indicating their chemical and physical stability - a crucial requirement for any potential uses.

Author Contributions: Conceptualization, S.S.; methodology, S.S.; validation, S.S., investigation, S.S., N.R,; writing—original draft preparation, S.S.; writing—review and editing, S.S.

Funding: This research was funded by the Ministry of Education, Science, and Technological Development of the Republic of Serbia (Grants 451-03-65/2024-03/ 200162 and 451-03-68/2023-14/200026) and by the European Union Horizon 2020 Research and Innovation program under the Marie Sklodowska-Curie grant agreement No. 823942 (FUNCOAT).

Data Availability Statement: The data presented in this study are available on request from the corresponding author.

Conflicts of Interest: The authors declare no conflict of interest.

References

1. Kaseem, M.; Fatimah, S.; Nashrah, N.; Ko, Y.G. Recent progress in surface modification of metals coated by plasma electrolytic oxidation: Principle, structure, and performance. Prog. Mater. Sci. **2021**, 117, 100735.
2. Simchen, F.; Sieber, M.; Kopp, A.; Lampke, T. Introduction to plasma electrolytic oxidation - an overview of the process and applications. Coatings **2020**, *10*, 628.
3. Tsai, D.-S.; Chou, C.-C. Review of the soft sparking issues in plasma electrolytic oxidation. Metals **2018**, *8*, 105.
4. Sikdar, S.; Menezes, P.V.; Maccione, R.; Jacob, T.; Menezes, P.L. Plasma electrolytic oxidation (PEO) process - processing, properties, and applications. Nanomaterials **2021**, *11*, 1375.
5. Clyne, T.W.; Troughton, S.C. A review of recent work on discharge characteristics during plasma electrolytic oxidation of various metals. Int. Mater. Rev. **2019**, *64*, 127–162.
6. Yang, Y.; Xiong, X.; Chen, J.; Peng, X.; Chen, D.; Pan, F. Research advances of magnesium and magnesium alloys worldwide in 2022. J. Magnes. Alloys **2023**, *11*, 2611–2654.
7. Tan, J.; Ramakrishna, S. Applications of magnesium and its alloys: a review, Appl. Sci. **2021**, *11*, 6861.
8. Esmaily, M.; Svensson, J.E.; Fajardo, S.; Birbilis, N.; Frankel, G.S.; Virtanen, S.; Arrabal, R.;0 Thomas, S.; Johansson, L.G. Fundamentals and advances in magnesium alloy corrosion. Prog. Mater. Sci. **2017**, *89*, 92–193.
9. Gray, J.E.; Luan, B. Protective coatings on magnesium and its alloys - a critical review. J. Alloys Compd. **2002**, *336*, 88–113.
10. Zhao, C.; Wang, X.; Yu, B.; Cai, M.; Yu, Q.; Zhou, F. Research progress on the wear and corrosion resistant plasma electrolytic oxidation composite coatings on magnesium and its alloys, Coatings **2023**, *13*, 1189.

11. Darband, Gh.B.; Aliofkhazraei, M.; Hamghalam, P.; Valizade, N. Plasma electrolytic oxidation of magnesium and its alloys: Mechanism, properties and applications, J. Magnes. Alloys **2017**, *5*, 74–132
12. Whitea, L.; Koo, Y.; Neralla, S.; Sankar, J.; Yun, Y. Enhanced mechanical properties and increased corrosion resistance of a biodegradable magnesium alloy by plasma electrolytic oxidation (PEO), Mater. Sci. Eng. B **2016**, *208*, 39–46.
13. Usmaniya, N.; Pillai, S.R.; Edalacheruvu, L.; Palanivel, M.; Chennampalli, P.; Vaithiyanathan, P.; Parfenov, E.; Lingamaneni, R.K.; Nagumothu, R. Effect of polycaprolactone coating on the corrosion and biological characteristics of plasma electrolytic oxidised ZM21 magnesium alloy. Surf. Coat. Technol. **2023**, *471*, 129915.
14. Fattah-alhosseini, A.; Molaei, M.; Nouri, M.; Babaei, K. Antibacterial activity of bioceramic coatings on Mg and its alloys created by plasma electrolytic oxidation (PEO): A review. J. Magnes. Alloys **2022**, *10*, 81–96.
15. Kumara, S.; Katyala, P.; Chaudhary, R.N.; Singh, V. Assessment of factors influencing bio-corrosion of magnesium based alloy implants: A review. Mater. Today Proc. **2022**, *56*, 2680–2689.
16. Kröger, N.; Kopp, A.; Staudt, M.; Rusu, M.; Schuh, A.; Liehn, E.A. Hemocompatibility of plasma electrolytic oxidation (PEO) coated Mg-RE and Mg-Zn-Ca alloys for vascular scaffold applications. Mater. Sci. Eng. C **2018**, *92*, 819–826.
17. Husak, Y.; Olszaniecki, J.; Pykacz, J.; Ossowska, A.; Blacha-Grzechnik, A.; Waloszczyk, N.; Babilas, D.; Korniienko, V.; Varava, Y.; Diedkova, K.; Kyrylenko, S.; Hodzic, A.; Krichbaum, M.; Lu, X.; Dryhval, B.; Pogorielov, M.; Simka, W. Influence of silver nanoparticles addition on antibacterial properties of PEO coatings formed on magnesium. Appl. Surf. Sci. **2024**, *654*, 159387.
18. Patrascu, I.; Ducu, M.C.; Negrea, A.D.; Moga, S.G.; Plaiasu. A.G. Overview on plasma electrolytic oxidation of magnesium alloys for medical and engineering applications. IOP Conf. Series: Mater. Sci. Eng. **2022**, *1251*, 012001.
19. Tang, M.; Li, G.; Li, W.; Liu, H.; Zhu. L. Photocatalytic performance of magnesium alloy microarc oxides. J. Alloys Compod **2013**, *562*, 84–89.
20. Li, W.; Tang, M.; Zhu. L.; Liu, H. Formation of microarc oxidation coatings on magnesium alloy with photocatalytic performance. Appl. Surf. Sci. **2012**, *258*, 10017–10021.
21. Stojadinović, S.; Tadić, N.; Radić, N.; Grbić, B.; Vasilić, R. MgO/ZnO coatings formed on magnesium alloy AZ31 by plasma electrolytic oxidation: Structural, photoluminescence and photocatalytic investigation. Surf. Coat. Technol. **2017**, *310*, 98–105.
22. Stojadinović, S.; Radić, N.; Vasilić, R. ZnO particles modified MgAl coatings with improved photocatalytic activity formed by plasma electrolytic oxidation of AZ31 magnesium alloy in aluminate electrolyte. Catalysts **2022**, *12*, 1503.
23. Stojadinović, S.; Radić, N.; Vasilić, R. Photoluminescent and photocatalytic properties of Eu^{3+}-doped MgAl oxide coatings formed by plasma electrolytic oxidation of AZ31 magnesium alloy. Coatings **2022**, *12*, 1830.
24. Supin, K.K.; Saji, A.; Chanda, A.; Vasundhara, M. Effects of calcinations temperatures on structural, optical and magnetic properties of MgO nanoflakes and its photocatalytic applications. Opt. Mater. **2022**, *132*, 112777.
25. Nitha, T.V.; Britto, S. MgAl2O4 nanospinel: Green synthesis, characterization and effective heterogeneous catalyst for the photocatalytic degradation of carbol fuchsin dye and synthesis of 2-aryl substituted benzoxazole derivatives. Inorg. Chem. Commun. **2024**, *159*, 111776.
26. Kiran, N.; Baker, A.P.; Wang, G.-G. Synthesis and luminescence properties of MgO:Sm^{3+} phosphor for white light-emitting diodes. J. Mol. Struct. **2017**, *1129*, 211–215.
27. Kumar, K.G. Bhargav, P.B.; Aravinth, K.; N. Ahmed, N.; Balaji, C. Photoluminescence and electrochemical performance evaluation of Eu^{3+} doped $MgAl_2O_4$ phosphors for LED and energy storage applications. Ceram. Int. **2022**, *48*, 36038–36045.
28. Mohedano, M.; Blawert, C.; Zheludkevich, M. L. Silicate-based plasma electrolytic oxidation (PEO) coatings with incorporated CeO2 particles on AM50 magnesium alloy. Mater. Des. **2015**, *86*, 735–744.
29. Lim, T.S.; Ryu, H.S.; Hong, S.-H. Electrochemical corrosion properties of CeO_2-containing coatings on AZ31 magnesium alloys prepared by plasma electrolytic oxidation. Corros. Sci. **2012**, *62*, 104–111.
30. Pan, J. Wang, S.; Chen, A.; Chen, Y.; Wang, M.; Chen, Y. Visible-light-active mesoporous ceria (CeO_2) nanospheres for improved photocatalytic performance, J. Alloys Compd. **2022**, *898*, 162895.
31. Kusmierek, E. A CeO2 semiconductor as a photocatalytic and photoelectrocatalytic material for the remediation of pollutants in industrial wastewater: a review. Catalysts **2020**, *10*, 1435.
32. Pudukudy, M.; Jia, Q.; Yuan, J.; Megala, S.; Rajendran, R.; Shan, S. Influence of CeO_2 loading on the structural, textural, optical and photocatalytic properties of single-pot sol-gel derived ultrafine CeO_2/TiO_2 nanocomposites for the efficient degradation of tetracycline under visible light irradiation. Mater. Sci. Semicond. Process. **2020**, *108*, 104891.
33. Habib, I.Y.; Burhan, J.; Jaladi, F.; Lim, C.M.; Usman, A.; Kumara, N.T.R.N.; Tsang, S.C.E.; Mahadi, A.H. Effect of Cr doping in CeO_2 nanostructures on photocatalysis and H_2O_2 assisted methylene blue dye degradation. Catal. Today **2021**, *375*, 506–513.

 doi:10.20944/preprints202403.0154.v1

34. Salimi, K. Self-assembled bio-inspired Au/CeO_2 nano-composites for visible white LED light irradiated photocatalysis. Colloids Surf. A **2020**, *559*, 124908
35. Wang, S.; Gao, H.; Li, J.; Wang, Y.; Chen, C.; Yu, X.; Tang, S.; Zhao, X.; Sun, G.; Li, D. Comparative study of the photoluminescence performance and photocatalytic activity of CeO_2/$MgAl_2O4$ composite materials with an n-n heterojunction prepared by one-step synthesis and two-step synthesis methods. J. Phys. Chem. Solids **2021**, *150*, 109891.
36. Matsukevich, I.; Kulinich, N.; Kulbitskaya, L.; Kuznetsova, T.; Popkov, V.; Chebanenko, M.; Moskovskikh, D.; Kuskov, K.; Romanovski, V. Mesoporous nanocomposites based on CeO_2 and MgO: preparation, structure and photocatalytic activity. J. Chem. Technol. Biotechnol. **2023**, *98*, 2497–2505.
37. Hoque, K.A.; Kumer, A.; Chakma, U.; Chowdhury, A.-N. Facile Synthesis of computationally designed $MgAl_2O_4$/CeO_2/Cu_2O and $MgAl_2O_4$/CeO_2/Ag_2O smart heterojunction photocatalysts for aqueous organic pollutants degradation. ECS Trans. **2022**, *107*, 13785–13796.
38. Stojadinović, S.; Radić, N.; Perković, M. Highly efficient ZrO_2 photocatalysts in the presence of UV radiation synthesized in a very short time by plasma electrolytic oxidation of zirconium. Opt. Mater. **2023**, *146*, 114608.
39. Rakoch, A.G.; Monakhova, E.P.; Khabibullina, Z.V.; Serdechnova, M.; Blawert, C.; Zheludkevich, M.L.; Gladkova, A.A. Plasma electrolytic oxidation of AZ31 and AZ91 magnesium alloys: Comparison of coatings formation mechanism. J. Magnes. Alloys 2020, 8, 587–600.
40. Zimou, J.; Nouneh, K.; Hsissou, R.; El-Habib, A.; El Gana, L.; Talbi, A.; Beraich, M.; Lotfi, N.; Addou, M. Structural, morphological, optical, and electrochemical properties of Co-doped CeO_2 thin films, Mater. Sci. Semicond. Process. **2021**, *135*, 106049.
41. Lua, X.; Mohedano, Ma.; Blawerta, C.; Matykina, E.; Arrabal, R.; Kainer, K.U.; M.L. Zheludkevich, Plasma electrolytic oxidation coatings with particle additions– A review. Surf. Coat. Technol. **2016**, *307*, 1165–1182.
42. Orsetti, F.R.; Bukman, L.; Santos, J.S.; Nagay, B.E.; Rangel, E.C.; Cruz, N.C. Methylene blue and metformin photocatalytic activity of CeO_2-Nb_2O_5 coatings is dependent on the treatment time of plasma electrolytic oxidation on titanium. Appl. Surf. Sci. Adv. **2021**, *6*, 100143.
43. Pathak, N.; Ghosh, P.S.; Gupta, S.K.; Mukherjee, S.; Kadam, R.M.; Arya, A. An insight into the various defects induced emission in $MgAl_2O_4$ and their tunability with phase behavior: Combined experimental and theoretical approach. J. Phys. Chem. C **2016**, *120*, 4016−4031.
44. Choudhuryn, B.; Basyach, P.; Choudhury, A. Monitoring F, F^+, and F_2^{2+} related intense defect emissions from nanocrystalline MgO, J. Lumin. **2014**, *149*, 280–286.
45. Pathak, N.; Ghosh, P.S.; Gupta, S.K.; Kadam, R.M.; Arya, A. Defects induced changes in the electronic structures of MgO and their correlation with the optical properties: a special case of electron–hole recombination from the conduction band. RSC Adv. **2016**, *6*, 96398.
46. Stojadinović, S.; Tadić, Radić, N.; Grbić, B.; Vasilić, R. MgO/ZnO coatings formed on magnesium alloy AZ31 by plasma electrolytic oxidation: Structural, photoluminescence and photocatalytic investigation. Surf. Coat. Technol. **2017**, *310*, 98–105.
47. Zhang, J.; Zhang, L. Intensive green light emission from MgO nanobelts. Chem. Phys. Lett. **2002**, *363*, 293–297.
48. Li, M.; Wang, X.; Li, H.; Di, H.; Wu, X.; Fang, C.; Yang, B. Preparation of photoluminescent single crystalline MgO nanobelts by DC arc plasma jet CVD. Appl. Surf. Sci. **2013**, *274*, 188–194.
49. Uchino, T.; Okutsu, D.; Katayama, R.; Sawai, S. Mechanism of stimulated optical emission from MgO microcrystals with color centers. Phys. Rev. B **2009**, *79*, 165107.
50. Lente, G. Facts and alternative facts in chemical kinetics: remarks about the kinetic use of activities, termolecular processes, and linearization techniques, Curr. Opin. Chem. Eng. **2018**, *21*, 76–83.
51. Fauzi, A.A.; Jalil, A.A.; Hassan, N.S.; Aziz, F.F.A.; Azami, M.S.; Hussain, I.; Saravanan, R.; Vo, D.-V.N. A critical review on relationship of CeO_2-based photocatalyst towards mechanistic degradation of organic pollutant. Chemosphere **2022**, *286*, 131651.
52. Liqiang, J.; Yichun, Q.; Baiqi, W.; Shudan, L.; Baojiang, J.; Libin, Y.; Wei, F.; Honggang, F.; Jiazhong, S. Review of photoluminescence performance of nano-sized semiconductor materials and its relationships with photocatalytic activity. Sol. Energy Mater. Sol. Cells **2006**, *90*, 1773–1787.